


Confinement effects on the random sequential adsorption packings of elongated particles in a slitNikolai I. Lebovka ^{1,*}, Mykhailo O. Tatchenko ^{1,†}, Nikolai V. Vygornitskii ^{1,‡} and Yuri Yu. Tarasevich ^{2,§}¹Laboratory of Physical Chemistry of Disperse Minerals,

F. D. Ovcharenko Institute of Biocolloidal Chemistry, NAS of Ukraine, Kyiv 03142, Ukraine

²Laboratory of Mathematical Modeling, Astrakhan State University, Astrakhan 414056, Russia (Received 22 July 2021; revised 9 September 2021; accepted 22 October 2021; published 8 November 2021)

The behavior of a system of two-dimensional elongated particles (discorectangles) packed in a slit between the two parallel walls was analyzed using a simulation approach. The packings were produced using the random sequential adsorption model with continuous positional and orientational degrees of freedom. The aspect ratio (length-to-width ratio, $\varepsilon = l/d$) of the particles was varied within the range $\varepsilon \in [1; 32]$ while the distance between the walls was varied within the range $h/d \in [1; 80]$. The properties of deposits in jammed state [the coverage, the order parameter, and the long-range (percolation) connectivity between particles] were studied numerically. The values of ε and h significantly affected the structure of the packings and the percolation connectivity. Particularly, the observed nontrivial dependencies of the jamming coverage $\varphi(\varepsilon)$ or $\varphi(h)$ were explained by the interplay of the different geometrical factors related to confinement, particle orientation degrees of freedom and excluded volume effects.

DOI: [10.1103/PhysRevE.104.054104](https://doi.org/10.1103/PhysRevE.104.054104)**I. INTRODUCTION**

In recent years, the different self-assemblies in random packings of elongated particles onto the two-dimensional (2D) substrates have attracted great attention [1]. Such assemblies may have attractive practical applications in memory devices, preparation of substrates with controlled wettability, transparent electrodes for optoelectronics, and sensing materials [2,3].

Self-assembly can be manifested in random sequential adsorption (RSA) process consisting in irreversible deposition of immobile particles onto a 2D substrate [4–6]. In the RSA process, the particles are deposited sequentially, their overlapping is forbidden, and above the saturated coverage concentration (“jamming limit”) the deposition process is terminated. For disks, the following values were obtained for saturated coverage: $\varphi = 0.5472 \pm 0.0002$ [7,8], $\varphi = 0.5470735 \pm 0.0000028$ [9], and $\varphi = 0.547067 \pm 0.000003$ [10]. This value is noticeably smaller than maximum packing fraction for close-packed configuration of disks, $\pi/\sqrt{12} \approx 0.9069$ [11]. Moreover, the RSA configuration is not stable since some disks may be rearranged to create holes sufficiently large to accommodate new disks [8].

For elongated particles, the RSA is a challenging problem that has been the ongoing focus of many researchers. The RSA packings of ellipses [12,13], rectangles [14,15], discorectangles [16,17], and other elongated objects [6,18–23] with the different values of the aspect ratio (length-to-

width ratios $\varepsilon = l/d$) have been analyzed. In many cases, the intriguing nonmonotonic $\varphi(\varepsilon)$ dependencies were observed. Such behavior was explained by a competition between the effects of orientational degrees of freedom and excluded area effects [24].

The spatially confined systems are of special interest for analysis of the effects of particle shape and extent of confining on particle self-assembly. The confinement effects have been extensively studied in equilibrium 2D systems enclosed between the two parallel hard walls (slit) and in the square or circular cavities [25–33]. The systems of particles with different geometries (ellipses, discorectangles, and rectangles) have been also analyzed [34]. Particularly, the surface phase diagram of a 2D hard-rectangle fluid confined between two walls was calculated [35]. A capillary columnar ordering and layering transitions in this system were observed. The density and the order-parameter profiles were calculated and formation of stationary texture consisting of layers of particles oriented parallel to the wall was demonstrated. Monte Carlo simulation of a system of hard rectangles confined between two walls was performed [36]. It was shown that confined particles tend to align their long axes parallel to the confining walls and the effects were more pronounced for small separation between the confining walls.

The strongly confined systems between the two parallel walls were theoretically examined for rectangular particles [37–39]. The density profiles shown planar ordering and damped oscillatory behavior [37]. For nonmesogenic particles with small values of the aspect ratio ($\varepsilon < 3$) in the extreme confinement limit, for small distances between walls ($h/d \leq 2$), a structural transition from a planar (particle’s long axis parallel to the walls) to a homeotropic (particle’s long axis perpendicular to the walls) layer with increasing density was observed [39]. For hard discorectangles between the two

*Corresponding author: lebovka@gmail.com

†tatchenkomiail@gmail.com

‡vygornv@gmail.com

§Corresponding author: tarasevich@asu.edu.ru

parallel walls in strongly confined systems ($1 < h/d \leq 2$), a rich phase behavior in dependence of the value of the particles' aspect ratio was observed [40]. For hard ellipses in a circular cavity, the formation of oriented layers in the vicinity of the wall was also reported [41].

For the case of the confined RSA system, we are only aware of the study of RSA configurations of hard disks with diameter d in narrow slit of width h ($1 < h/d < 2$) [42]. The case $h = d$ corresponds to the 1D packing of disks onto the line. Jamming coverage for parking of 1D segments of the same length onto the line was exactly evaluated to be about $\varphi_R = 0.7476\dots$ (Rényi's parking constant) [43].

For 1D RSA disk systems, it gives $\varphi = (\pi/4)\varphi_R \approx 0.5872$. With an increase of h value, there was observed a noticeable decrease of φ value. However, to our best knowledge, the confined RSA system with elongated particles were never studied before.

The present work deals with 2D RSA packings of elongated particles (discorectangles) in confined geometry between the two parallel plates (a slit). The computationally efficient technique to generate jamming configurations was employed. The observed orientational structures of packings evidenced on presence of ordering inside slit. Mean values of the coverage $\varphi(\varepsilon)$ and the order parameter S demonstrated nonmonotonic behavior in dependence on ε and h . Connectivity of particles with hard core–soft shell structure was also analyzed. The rest of the paper is organized as follows. In Sec. II, the technical details of the simulations are described and all necessary quantities are defined. Section III presents our principal findings and discussions. Finally, Sec. IV presents some concluding remarks.

II. COMPUTATIONAL MODEL

The elongated particles were represented by the hard discorectangles, which consist of a rectangular part (length l and width d) with two semicircular caps of diameter d at its opposite ends. To simplify presentation, in further consideration, all lengths are given in units of d . The particles with $\varepsilon \in [1; 32]$ were analyzed. The RSA model was used for formation of packings. The particles with random orientations were randomly and sequentially deposited into a slit (in the space between the two parallel impenetrable walls with the distance h between them). Overlapping of a particle with the previously deposited ones and with the walls was strictly forbidden (Fig. 1). In the jamming state no additional particle can be added to the system due to the absence of a pore with appropriate size. The closest distance of approach of a particle to any of the walls was 0.5.

The computationally efficient technique to generate jamming configurations, based on the tracking of local regions, was employed [16,17]. The saturated coverage was evaluated as $\varphi = NA_p/A$, where N is a number of deposited particles, and A_p and A are the area of a particle and a slit, correspondingly. In the following discussion, the properties of systems in the jamming state will be only analyzed.

The width of a slit was varied within $h \in [1; 80]$ and periodic boundary conditions (PBCs) were used in the vertical (y) direction. The length of the slit in the vertical (y) direction

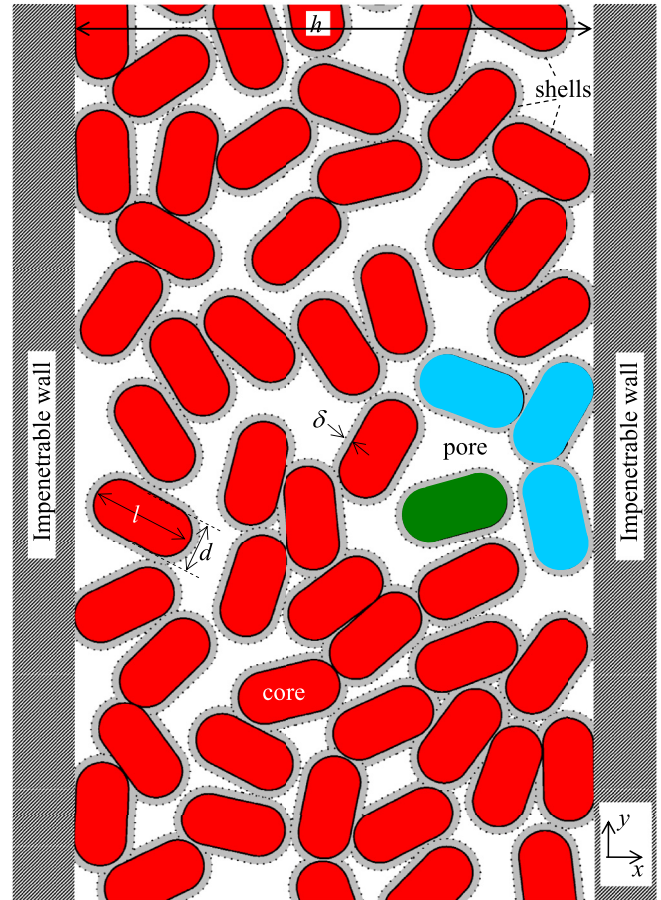


FIG. 1. A schematic picture of the of RSA packing of elongated particles between the two parallel walls with the distance h between them. The walls and particles (cores) are assumed to be impenetrable. The cores of particles are discorectangles with the length l and width d . The space between particles can be treated as pores. Periodic boundary conditions are applied in y direction. For connectivity analysis along the x and y axes, the particles were covered with shells of thickness δ . The particles of different shades correspond to the different clusters.

was L . In the present work, the majority of calculations were performed using $L = 16384$ (see some scaling tests in Appendix A). The comparative data to mimic infinite systems were obtained using PBCs applied in both the horizontal (x) and the vertical (y) directions with the systems size $32\varepsilon \times 32\varepsilon$ (more detailed information can be found elsewhere [23]).

For connectivity analysis along x and y axes, a core-shell structure of the particles was assumed. The particle cores were covered with shells of thickness δ (Fig. 1). The minimum thickness of overlapping shells, required for the formation of spanning clusters in the x or y direction, was determined using a list of near-neighbor particles [44] and the Hoshen-Kopelman algorithm [45].

During the deposition of particles with random orientations in a confined slit, some attempts of particle deposition may be rejected due to the intersection with walls. The preliminary studies demonstrated that, in a confined slit, the aligned packings with preferred orientation along slit (y direction) are formed. Moreover, for conditions with strong confinement at

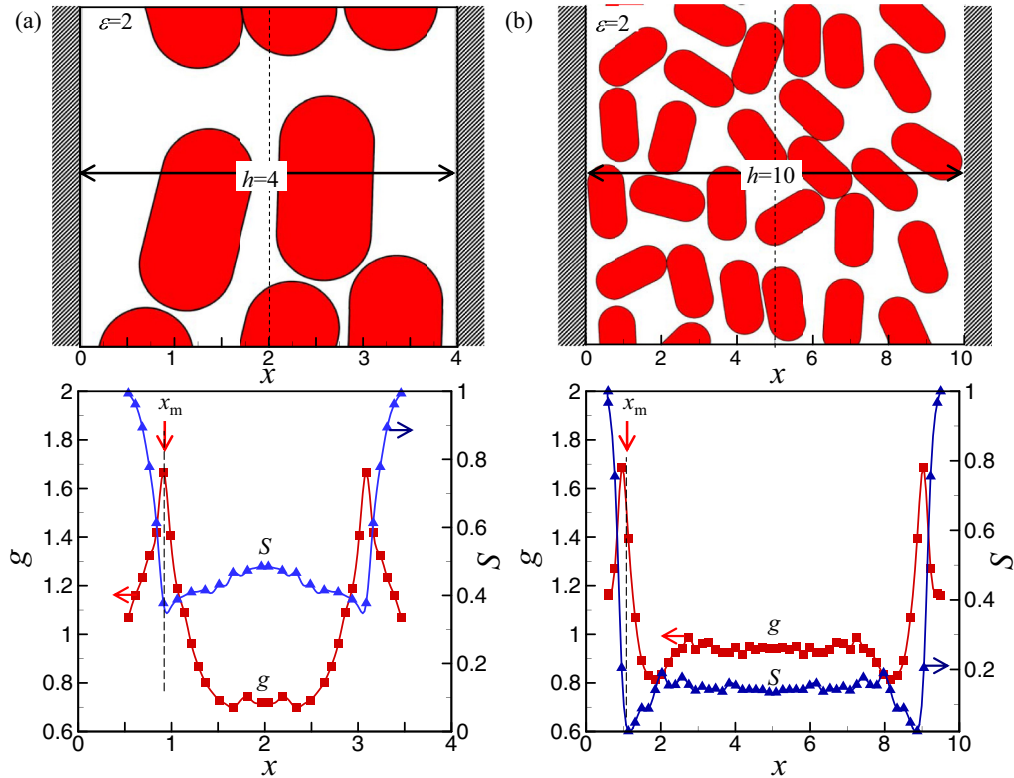


FIG. 2. Examples of packing patterns (top), and profiles of the scaled coverage $g(x) = \varphi(x)/\langle\varphi\rangle$ and the order parameter, $S(x)$ (bottom), for the value of the aspect ratio $\varepsilon = 2$ and the distance between walls $h = 4$ (a) and $h = 10$ (b). The corresponding mean values, averaged through the slit, are $\langle\varphi\rangle = 0.518 \pm 0.01$ and $\langle S\rangle = 0.54 \pm 0.01$ (a) and $\langle\varphi\rangle = 0.558 \pm 0.01$ and $\langle S\rangle = 0.26 \pm 0.01$ (b). Here x_m corresponds to the positions of the extremum in $\varphi^*(x)$ (maxima) or $S(x)$ (minima) dependencies.

rather small value of the slit width $h \leq 2$, the “defective” packings with diminished density were observed due to the commensuration effect between the width of the particle and the wall separation.

The degree of orientation in the formed aligned packing was characterized by the order parameter defined as

$$S = \langle \cos 2\theta \rangle, \quad (1)$$

where $\langle \cdot \rangle$ denotes the average and θ is the angle between the long axis of the particle and the axis y .

Profiles of the local coverage $\varphi(x)$ and the order parameter $S(x)$ were calculated as an ensemble average of the particles that have their centers of mass at a distance from the wall between x and $x + dx$. Typically, in our calculations, we have used $dx = 0.05$ – 0.1 .

For each given value of ε and h , the computer experiments were repeated from 10 to 100 independent packings. The error bars in the figures correspond to the standard deviations of the means. When not shown explicitly, they are of the order of the marker size.

III. RESULTS AND DISCUSSION

Figure 2 demonstrates examples of packing patterns (top), and profiles of the scaled coverage $g(x) = \varphi(x)/\langle\varphi\rangle$ and the order parameter $S(x)$ (bottom) for the value of the aspect ratio $\varepsilon = 2$ and the distance between walls $h = 4$ (a) and $h = 10$

(b). Here $\langle\varphi\rangle$ is the mean value of the coverage, averaged through the slit.

The oscillating profiles of $g(x)$ and $S(x)$ were observed for other values of ε and h (see Appendix B). Obtained data evidenced that hard walls induced formation of layers of particles in the vicinity of walls when particles’ long axes are preferred aligned parallel to the walls. Both the profiles were symmetric with respect to a line at the center of the slit.

The similar profiles were captured by both simulations and theories for equilibrium systems of particles confined between parallel hard walls with varying widths, h . For example, in three-dimensional confined geometries between parallel walls, the oscillatory behavior of the local density were observed for hard spheres [46], spherocylinders [47–50], rod-like particles [51], cylinders [52], and rectangular rods [53]. Strong structuration of the systems near the walls, and different confined isotropic, nematic, and smectic phases for elongated particles, were observed [49]. The similar effects were also observed in 2D confined geometries between parallel hard walls for ellipses, discorctangles, and rectangles [34–36,53].

It is remarkable that, for the selected value of $\varepsilon = 2$ (Fig. 2), the coverage and the order parameter profiles revealed the distinctive peak at a distance of about width of the particle ($x_m \approx 1$) from the wall surface. In the general case, the positions of the first maximum in $g(x)$ dependency and the first minimum in $S(x)$ were observed at nearly the same distance from the wall, x_m . The value of x_m may be identified

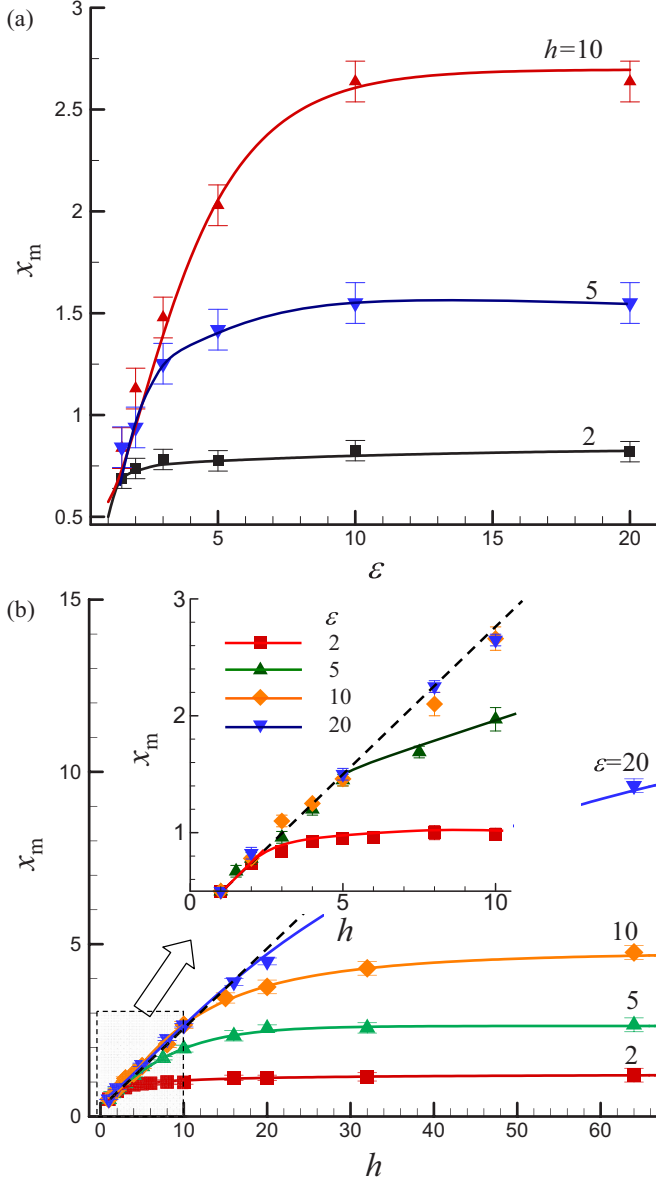


FIG. 3. Position of the extremum x_m in spatial distribution of the coverage φ or the order parameter S versus the aspect ratio ε in a slit with different distances between walls h (a) and x_m versus h at different values of ε (b). Inset shows the enlarged part of $x_m(h)$ dependence (b).

with surface layer thickness. Figure 3 presents dependencies of the thickness x_m versus ε at different values of h (a) and x_m versus h at different values of ε (b). At a fixed value of h , the thickness x_m initially increased with ε and saturated for long particles with large values of ε [Fig. 3(a)]. In particular, the saturated values of x_m were ≈ 0.83 at $h = 2$, ≈ 1.54 at $h = 5$, and ≈ 2.56 at $h = 10$. Similarly, at a fixed value of ε , the thickness x_m initially increased with h and then saturated for larger values of h [Fig. 3(b)]. The dashed line in Fig. 3(b) corresponds to the linear dependence $x_m = 0.25(1 + h)$. This linear increase of the surface layer thickness with h was only observed in strongly confined systems with $h \leq \varepsilon$ [see inset Fig. 3(b)], while at larger values of h , the transition to

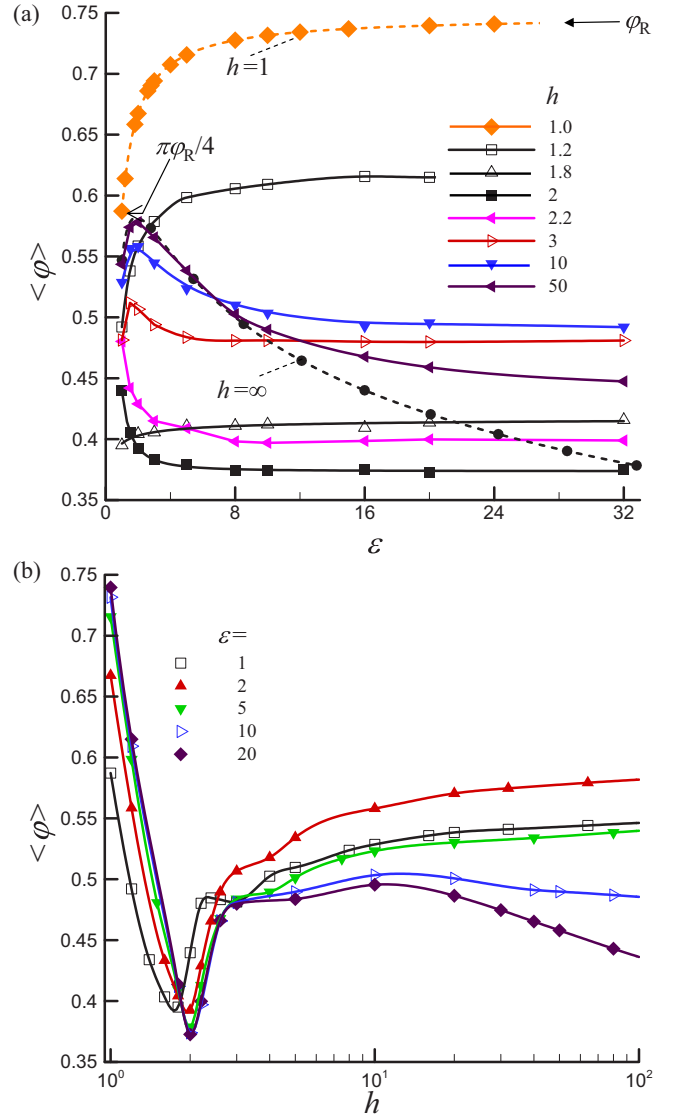


FIG. 4. The mean coverage $\langle \varphi \rangle$ versus the aspect ratio ε in slits with different distances h between the walls (a) and versus the h for different values of ε (b).

saturated behavior of $x_m(h)$ was observed. Therefore, in confined systems the extent of perturbation induced by walls depends on the interrelation between the wall-to-wall distance and length of the particle.

Figure 4 presents the mean coverage $\langle \varphi \rangle$ versus the aspect ratio ε in slits with different distances h between the walls (a) and versus the h for different values of ε (b). For strongly confined 1D systems ($h = 1$), the dependence $\langle \varphi(\varepsilon) \rangle$ may be calculated as

$$\langle \varphi \rangle = \varphi_R \frac{\pi/4 + \varepsilon - 1}{\varepsilon}, \quad (2)$$

where $\varphi_R = 0.7476\dots$ is the Rényi's parking constant [43]. The numerator $\pi/4 + \varepsilon - 1$ corresponds to the area of discorctangle (with length $l = \varepsilon$ and width $d = h = 1$). The denominator ε corresponds to the area of rectangle (with length $l = \varepsilon$ and width $d = h = 1$). This formula gives the dashed line for $h = 1$ presented in Fig. 4(a) with

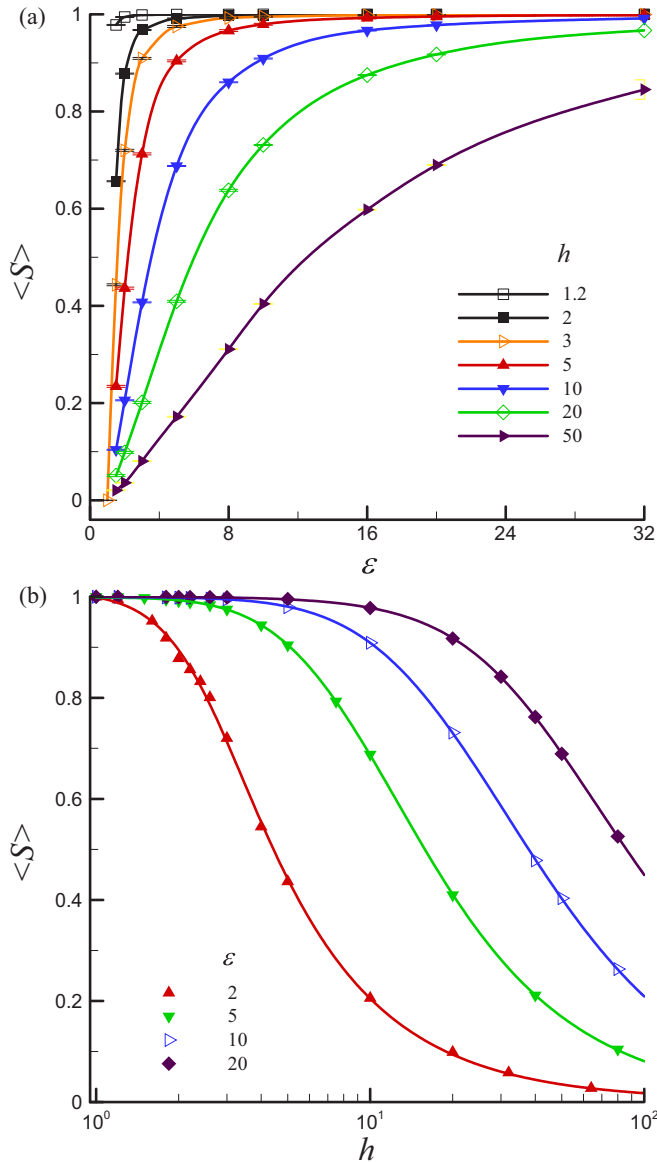


FIG. 5. The mean order parameter $\langle S \rangle$ versus the aspect ratio ε in slits with different distances h between the walls (a) and versus the h for different values of ε (b).

$\langle \varphi \rangle = (\pi/4)\varphi_R$ for disks ($\varepsilon = 1$) and $\langle \varphi \rangle = \varphi_R$ for infinitely long particles ($\varepsilon \rightarrow \infty$).

For 2D systems with $h > 1$, a wide variety of monotonic and nonmonotonic $\langle \varphi(\varepsilon) \rangle$ dependencies have been observed. Particularly, for the system with PBCs (the systems with size $32\varepsilon \times 32\varepsilon$ was used to imitate the infinitely large system) the maximum in $\langle \varphi(\varepsilon) \rangle$ dependence can be explained accounting for the competition between the particles' orientational degrees of freedom and excluded area effects [16,17,23].

The monotonic $\langle \varphi(\varepsilon) \rangle$ dependencies have been only observed in strongly confined systems with $h < 3$. Particularly, the confined systems with $h = 2$ demonstrated specific behavior with the smallest values of the coverage below $\langle \varphi \rangle \approx 0.4$ for $\varepsilon > 2$. However, for higher distances between wall ($h \geq 3$) the similar maximums in $\langle \varphi(\varepsilon) \rangle$ dependencies have been also detected [Fig. 4(a)]. Figure 4(b) presents

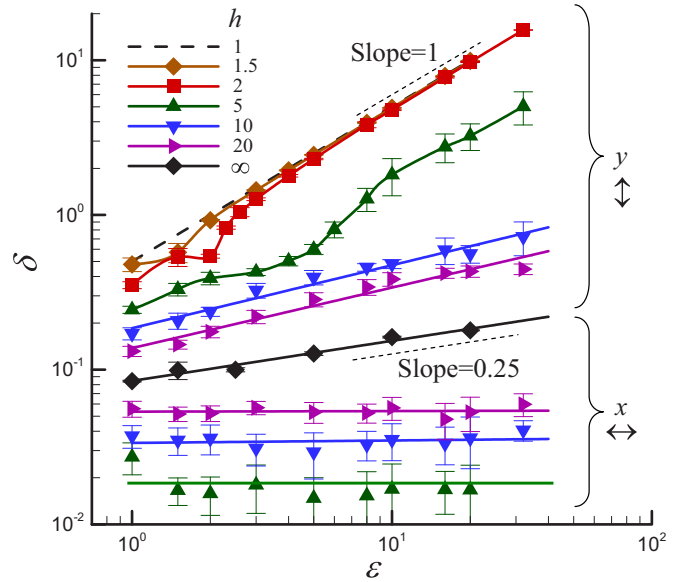


FIG. 6. Thickness of the connectivity shell δ versus the aspect ratio ε along $x(\leftrightarrow)$ and $y(\updownarrow)$ axes for different distances between walls h .

dependencies of the mean coverage $\langle \varphi \rangle$ versus the slit width h for particles with different values of the aspect ratio, ε . The dependencies $\langle \varphi(h) \rangle$ displayed the minimums at approximately the same $h \in [1.9, 2]$ for all studied values of the aspect ratio, ε [Fig. 4(a)]. Obtained data for disks ($\varepsilon = 1$) were in good agreement with previously reported data for the range $1 < h \leq 2$ [42]. Therefore, the RSA packing in slits revealed the extreme $\langle \varphi(\varepsilon) \rangle$ dependencies at $h > 3$ (maximums at $\varepsilon \in [1, 1.8]$) [Fig. 4(a)] and the extreme $\langle \varphi(h) \rangle$ dependencies at $h < 3$ (minimums at $h \approx 2$) [Fig. 4(b)].

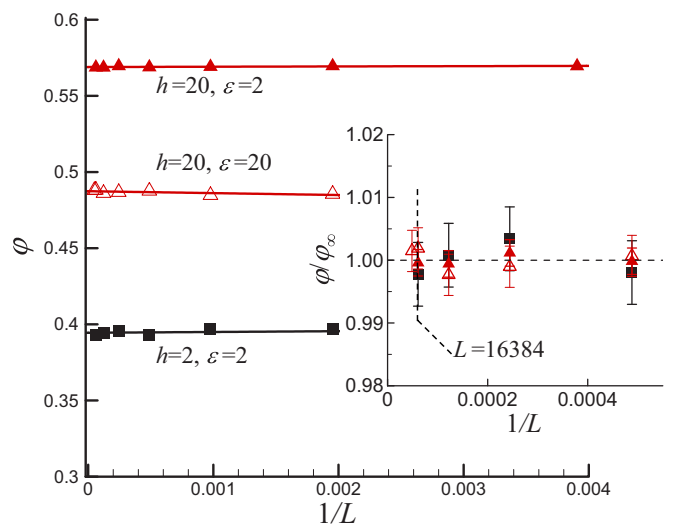


FIG. 7. Examples of the coverage φ versus the inverse length of a slit $1/L$ at different distances between its walls h and the aspect ratio of particles ε . Inset shows φ/φ_∞ versus $1/L$, where φ_∞ corresponds to the limit $L \rightarrow \infty$. The value of φ_∞ was determined using linear approximation for $\varphi(1/L)$ dependence.

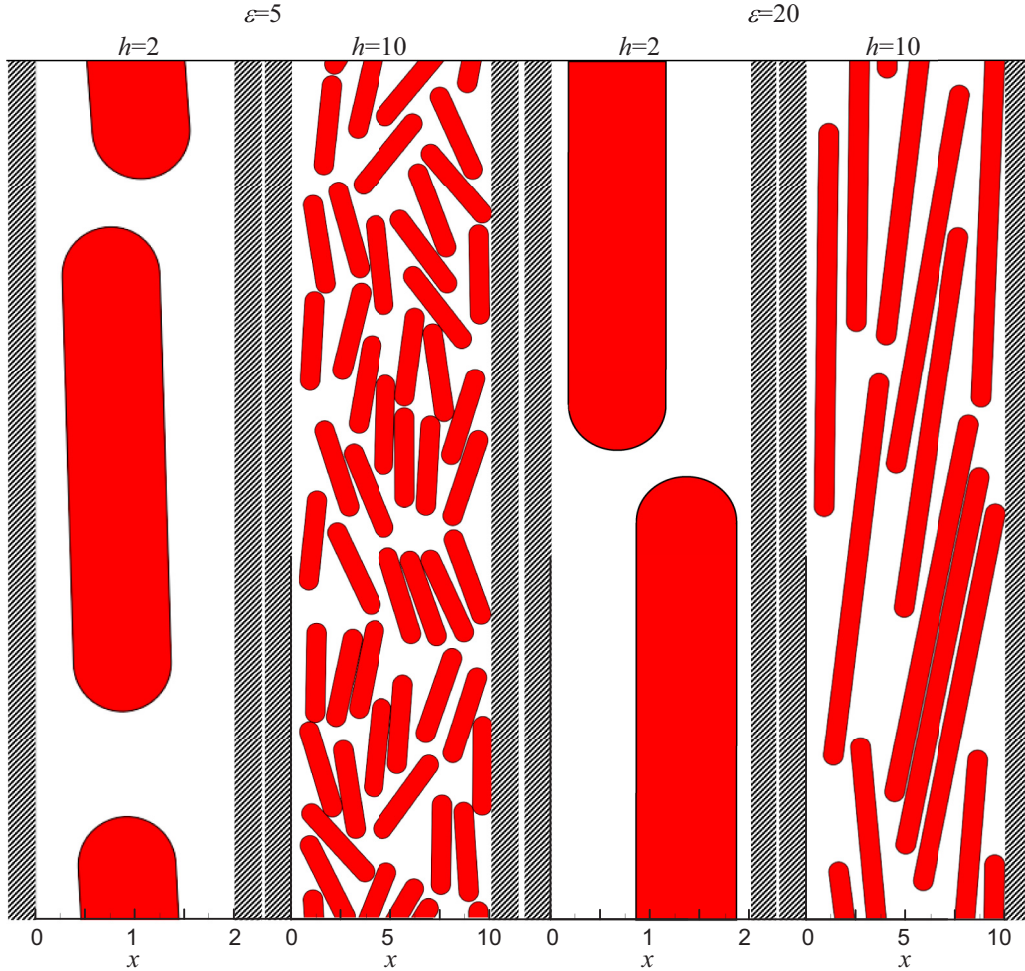


FIG. 8. Examples of the packing patterns for the values of the aspect ratios $\varepsilon = 5$ and $\varepsilon = 20$, and distances between the walls $h = 2$ and $h = 20$.

Note that in strongly confined systems ($1 < h \leq 2$) of discorightangles or ellipses, a rich phase behavior in dependence of the value of the particles' aspect ratio was recently reported [40,54]. For small values of the aspect ratio ($\varepsilon = 1 - 5$), the values of the mean coverage $\langle \varphi \rangle$ saturated at larger distances between walls ($h > 10$). However, for particles with large values of the aspect ratio ($\varepsilon \gtrsim 10-20$), the decrease in the mean coverage $\langle \varphi \rangle$ with increase values of h was observed for larger values of the distance between the walls ($h > 10-20$).

The dependencies $\langle S(\varepsilon) \rangle$ shown only monotonic character and order parameter was higher for thinner slit and increased with increase of ε [Fig. 5(a)]. This behavior reflected the presence of highly oriented layers of particles formed in the vicinity of both walls (Fig. 2). Therefore, confinement by walls resulted in adding of the supplementary lever into the competition between the particles' orientational degrees of freedom and excluded area effects. Moreover, at fixed values of ε , the values of $\langle S \rangle$ continuously decreased with increase values of h . The effects were more pronounced for particles with small values of the aspect ratio, ε [Fig. 5(b)].

Figure 6 presents the thickness of the connectivity shell δ versus the aspect ratio ε in directions across the horizontal axis $x(\leftrightarrow)$ and along the vertical axis $y(\updownarrow)$ for different distances

between walls, h . The values of δ for the horizontal axis $x(\leftrightarrow)$ were relatively small and independent on the aspect ratio ε .

Behavior of δ along the vertical axis $y(\updownarrow)$ was more complicated. For the 1D-confined system with $h = 1$, the linear dependence $\delta = 0.5\varepsilon$ along the $y(\updownarrow)$ axis was observed (dashed line with the slope equals to 1). For this case, the connectivity emerged at higher values for soft shell thickness around the particles. For strongly confined systems with $h = 1.5-5$, the dependencies $\delta(\varepsilon)$ revealed nonmonotonic anomalies with inflection points at small values of ε (Fig. 6). For larger distances between walls ($h \geq 10$), the powerlike dependencies $\delta \propto \varepsilon^\alpha$ with exponent $0.25 < \alpha < 1$. Finally, for imitated infinite systems (systems PBCs applied in both the horizontal (x) and the vertical (y) directions with the systems size $32\varepsilon \times 32\varepsilon$ [23]) the value $\alpha \approx 0.25$ was estimated. Obtained data evidenced that confinement between walls results in weakening of connectivity along the vertical axis $y(\updownarrow)$ and enhancing of it across the horizontal axis $x(\leftrightarrow)$.

IV. CONCLUSION

Numerical studies of two-dimensional RSA deposition of discorightangles confined between the two parallel walls (in

slit) were carried out. It was shown that the introduction of the confinement changed significantly the distribution of particles and their orientations inside the slit. Near the walls, the particles were mostly aligned parallel to the walls. The thickness of the surface layers and extent of the surface perturbation induced by the walls depend on the interrelation between the values of h and ε . The mean coverage $\langle\varphi\rangle$ and the mean order parameter $\langle S\rangle$ were also strongly dependent on the values of h and ε . Particularly, for finite values of h , the monotonic $\langle\varphi(\varepsilon)\rangle$ dependencies have been only observed in strongly confined systems with $h < 3$. However, for higher distances between the walls ($h \geq 3$), the maxima in $\langle\varphi(\varepsilon)\rangle$ dependencies have been also detected. Moreover, the minima in $\langle\varphi(h)\rangle$ dependencies at approximately the same values $h \approx 1.9-2$ for all studied values of the aspect ratio, ε , were observed. This behavior reflected the presence in confined systems of the supplementary lever into the competition between the particles' orientational degrees of freedom and excluded area effects. Obtained data also evidenced that the confinement between walls results in weakening of the connectivity along the walls and enhancing of it perpendicularly to walls.

Effects of confinements may be important in irreversible adsorption of particles (e.g., adsorption of macromolecules or colloidal particles onto chemically heterogeneous or morphologically irregular surfaces [55–57]). The studied RSA systems are nonequilibrium and their direct comparison with the thermally equilibrium systems requires additional

studies of relaxation effects during the transition from RSA to the equilibrium state. Such transition may be accompanied with noticeable effects on alignment of confined particles with their long axes being parallel to the confining walls in dependence on separation between the walls [36]. Future studies could generalize our approach to different anchoring interactions of particles with the walls and confinement in different geometries like circular or square cavities.

ACKNOWLEDGMENTS

We acknowledge funding from the National research foundation of Ukraine, Grant No. 2020.02/0138 (M.O.T. and N.V.V.); the National Academy of Sciences of Ukraine, Projects No. 7/9/3-f-4-1230-2020, No. 0120U100226, and No. 0120U102372/20-N (N.I.L.); and funding from the Foundation for Advancement of Theoretical Physics and Mathematics “BASIS,” Grant No. 20-1-1-8-1 (Y.Y.T.).

APPENDIX A: SCALING TESTS

The length of the slit in the vertical (y) direction was L . The scaling tests with $L = 2^n$, $n \in [8; 14]$ evidenced the good convergence of the data for the coverage φ (Fig. 7). Therefore, in the present work, the majority of calculations were performed using $L = 16384$, $n = 14$.

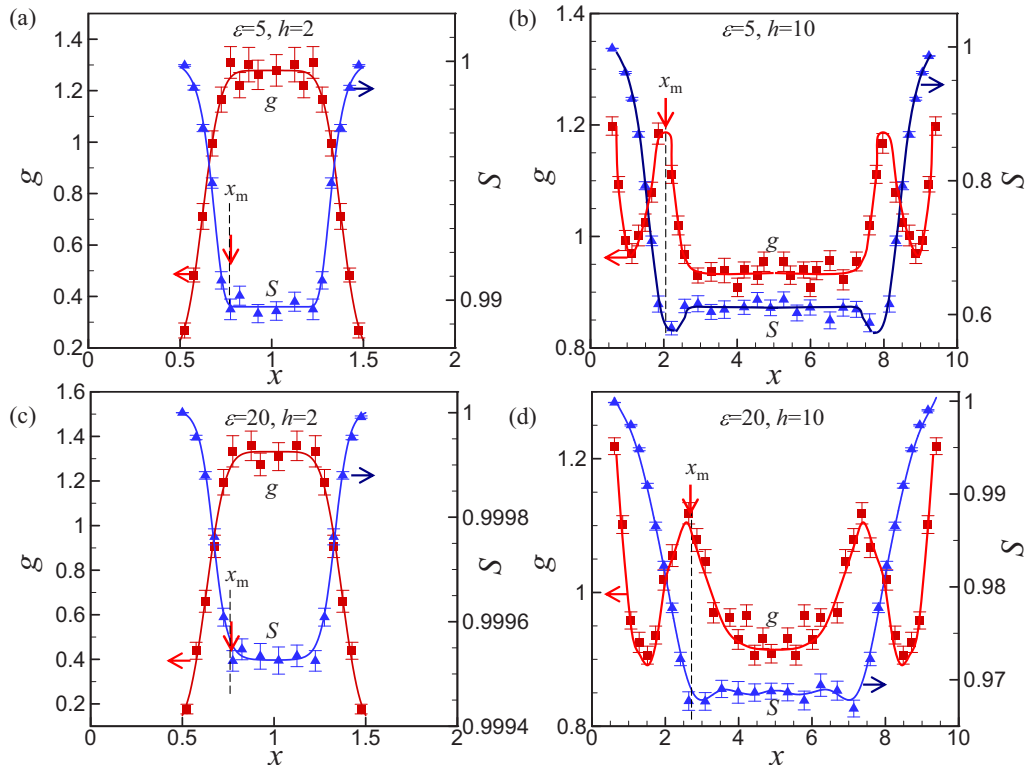


FIG. 9. Examples of the profiles of the scaled coverage $g(x) = \varphi(x)/\langle\varphi\rangle$ and the order parameter, $S(x)$ for the different values of the aspect ratio ε and distances between the walls h : $\varepsilon = 5$, $h = 2$ (a); $\varepsilon = 5$, $h = 10$ (b); $\varepsilon = 20$, $h = 2$ (c); and $\varepsilon = 20$, $h = 10$ (d). Here x_m corresponds to the positions of the extremum in the $g(x)$ (maxima) or $S(x)$ (minima) dependencies, and $\langle\varphi\rangle$ is the mean value of the coverage, averaged across the slit.

APPENDIX B: PROFILES OF THE SCALED COVERAGE AND THE ORDER PARAMETER

Figure 8 presents supplementary examples of the packing patterns for the values of the aspect ratios $\varepsilon = 5$ and $\varepsilon = 20$ and distances between the walls $h = 2$ and $h = 10$. In a strongly confined slits ($h = 2$) the aligned packings with preferred orientation along slit (y direction) are formed.

Figure 9 presents supplementary examples of the profiles of the scaled coverage $g(x) = \varphi(x)/\langle\varphi\rangle$ and the order parameter $S(x)$ for the different values of the aspect ratio ε and distances between the walls h : $\varepsilon = 5, h = 2$ (a); $\varepsilon = 5, h = 10$

(b); $\varepsilon = 20, h = 2$ (c); and $\varepsilon = 20, h = 10$ (d). Here $\langle\varphi\rangle$ is the mean value of the coverage, averaged across the slit. Note that in strongly confined slits ($h = 2$), the thickness of the aligned packings with preferred orientation along the slit (y axis) was nearly the same $x_m \approx 0.75$ for both the cases of $\varepsilon = 5$ and $\varepsilon = 20$. The values of $g(x)$ were maximal near the walls and minimal inside slits, while the behavior of the order parameter, $S(x)$, was inverse. However, in wider slits ($h = 10$), the oscillation behaviors of $g(x)$ and $S(x)$ were observed. In general case, dependencies of x_m on the values of ε and h are presented in Fig. 3.

-
- [1] O. Jahanmahin, D. J. Kirby, B. D. Smith, C. A. Albright, Z. A. Gobert, C. D. Keating, and K. A. Fichthorn, Assembly of gold nanowires on gold nanostripe arrays: Simulation and experiment, *J. Phys. Chem. C* **124**, 9559 (2020).
- [2] Z. Fang, Q. Xing, D. Fernandez, X. Zhang, and G. Yu, A mini review on two-dimensional nanomaterial assembly, *Nano Res.* **13**, 1179 (2020).
- [3] K. Deng, Z. Luo, L. Tan, and Z. Quan, Self-assembly of anisotropic nanoparticles into functional superstructures, *Chem. Soc. Rev.* **49**, 6002 (2020).
- [4] J. W. Evans, Random and cooperative sequential adsorption, *Rev. Mod. Phys.* **65**, 1281 (1993).
- [5] Z. Adamczyk, Modeling adsorption of colloids and proteins, *Curr. Opin. Colloid Interface Sci.* **17**, 173 (2012).
- [6] N. I. Lebovka and Y. Y. Tarasevich, Two-dimensional systems of elongated particles: From diluted to dense, in *Order, Disorder and Criticality. Advanced Problems of Phase Transition Theory*, Vol. 6, edited by Y. Holovatch (World Scientific, Singapore, 2020), pp. 30–60.
- [7] E. L. Hinrichsen, J. Feder, and T. Jøssang, Geometry of random sequential adsorption, *J. Stat. Phys.* **44**, 793 (1986).
- [8] E. L. Hinrichsen, J. Feder, and T. Jøssang, Random packing of disks in two dimensions, *Phys. Rev. A* **41**, 4199 (1990).
- [9] G. Zhang and S. Torquato, Precise algorithm to generate random sequential addition of hard hyperspheres at saturation, *Phys. Rev. E* **88**, 053312 (2013).
- [10] M. Cieřla and R. M. Ziff, Boundary conditions in random sequential adsorption, *J. Stat. Mech: Theory Exp.* (2018) 043302.
- [11] C. Zong, in *Sphere Packings*, edited by J. Talbot (Springer Science & Business Media, New York, 1999).
- [12] J. Talbot, G. Tarjus, P. R. Van Tassel, and P. Viot, From car parking to protein adsorption: An overview of sequential adsorption processes, *Colloids Surf., A* **165**, 287 (2000).
- [13] J. D. Sherwood, Random sequential adsorption of lines and ellipses, *J. Phys. A: Math. Gen.* **23**, 2827 (1990).
- [14] R. D. Vigil and R. M. Ziff, Random sequential adsorption of unoriented rectangles onto a plane, *J. Chem. Phys.* **91**, 2599 (1989).
- [15] R. D. Vigil and R. M. Ziff, Kinetics of random sequential adsorption of rectangles and line segments, *J. Chem. Phys.* **93**, 8270 (1990).
- [16] K. Haiduk, P. Kubala, and M. Cieřla, Saturated packings of convex anisotropic objects under random sequential adsorption protocol, *Phys. Rev. E* **98**, 063309 (2018).
- [17] N. I. Lebovka, N. V. Vygornitskii, and Y. Y. Tarasevich, Random sequential adsorption of partially ordered discorectangles onto a continuous plane, *Phys. Rev. E* **102**, 022133 (2020).
- [18] E. J. Perino, D. A. Matoz-Fernandez, P. M. Pasinetti, and A. J. Ramirez-Pastor, Jamming and percolation in random sequential adsorption of straight rigid rods on a two-dimensional triangular lattice, *J. Stat. Mech: Theory Exp.* (2017) 073206.
- [19] L. Budinski-Petković, I. Lončarević, Z. M. Jakšić, and S. B. Vrhovac, Jamming and percolation in random sequential adsorption of extended objects on a triangular lattice with quenched impurities, *J. Stat. Mech: Theory Exp.* (2016) 053101.
- [20] M. Cieřla and J. Barbasz, Modelling of interacting dimer adsorption, *Surf. Sci.* **612**, 24 (2013).
- [21] M. Cieřla, Continuum random sequential adsorption of polymer on a flat and homogeneous surface, *Phys. Rev. E* **87**, 052401 (2013).
- [22] M. Cieřla, G. Paja, and R. M. Ziff, Shapes for maximal coverage for two-dimensional random sequential adsorption, *Phys. Chem. Chem. Phys.* **17**, 24376 (2015).
- [23] N. I. Lebovka, M. O. Tatochenko, N. V. Vygornitskii, A. V. Eserkepov, R. K. Akhunzhanov, and Y. Y. Tarasevich, Connectedness percolation in the random sequential adsorption packings of elongated particles, *Phys. Rev. E* **103**, 042113 (2021).
- [24] A. Donev, I. Cisse, D. Sachs, E. A. Variano, F. H. Stillinger, R. Connelly, S. Torquato, and P. M. Chaikin, Improving the density of jammed disordered packings using ellipsoids, *Science* **303**, 990 (2004).
- [25] D. de las Heras, E. Velasco, and L. Mederos, Topological defects in a two-dimensional liquid crystal confined in a circular nanocavity, *Phys. Rev. E* **79**, 061703 (2009).
- [26] D. de las Heras, L. Mederos, and E. Velasco, Density-functional study of defects in two-dimensional circular nematic nanocavities, *Liq. Cryst.* **37**, 45 (2009).
- [27] J. Z. Y. Chen, Structure of two-dimensional rods confined by a line boundary, *Soft Matter* **9**, 10921 (2013).
- [28] M. González-Pinto, Y. Martínez-Ratón, and E. Velasco, Liquid-crystal patterns of rectangular particles in a square nanocavity, *Phys. Rev. E* **88**, 032506 (2013).
- [29] T. Geigenfeind, S. Rosenzweig, M. Schmidt, and D. de las Heras, Confinement of two-dimensional rods in slit pores and square cavities, *J. Chem. Phys.* **142**, 174701 (2015).

- [30] D. de las Heras and E. Velasco, Domain walls in two-dimensional nematics confined in a small circular cavity, *Soft Matter* **10**, 1758 (2014).
- [31] C. E. Sitta, F. Smallenburg, R. Wittkowski, and H. Löwen, Hard rectangles near curved hard walls: Tuning the sign of the Tolman length, *J. Chem. Phys.* **145**, 204508 (2016).
- [32] C. E. Sitta, F. Smallenburg, R. Wittkowski, and H. Löwen, Liquid crystals of hard rectangles on flat and cylindrical manifolds, *Phys. Chem. Chem. Phys.* **20**, 5285 (2018).
- [33] X. Yao, H. Zhang, and J. Z. Y. Chen, Topological defects in two-dimensional liquid crystals confined by a box, *Phys. Rev. E* **97**, 052707 (2018).
- [34] D. de las Heras, Y. Martínez-Ratón, L. Mederos, and E. Velasco, Two-dimensional nematics in bulk and confined geometries, *J. Mol. Liq.* **185**, 13 (2013).
- [35] Y. Martínez-Ratón, Capillary ordering and layering transitions in two-dimensional hard-rod fluids, *Phys. Rev. E* **75**, 051708 (2007).
- [36] D. A. Triplet and K. A. Fichtorn, Monte Carlo simulation of two-dimensional hard rectangles: Confinement effects, *Phys. Rev. E* **77**, 011707 (2008).
- [37] R. Aliabadi, M. Moradi, and S. Varga, Orientational ordering of confined hard rods: The effect of shape anisotropy on surface ordering and capillary nematization, *Phys. Rev. E* **92**, 032503 (2015).
- [38] P. Gurin, S. Varga, M. González-Pinto, Y. Martínez-Ratón, and E. Velasco, Ordering of hard rectangles in strong confinement, *J. Chem. Phys.* **146**, 134503 (2017).
- [39] R. Aliabadi, P. Gurin, E. Velasco, and S. Varga, Ordering transitions of weakly anisotropic hard rods in narrow slitlike pores, *Phys. Rev. E* **97**, 012703 (2018).
- [40] E. Basurto, P. Gurin, S. Varga, and G. Odriozola, Ordering, clustering, and wetting of hard rods in extreme confinement, *Phys. Rev. Res.* **2**, 013356 (2020).
- [41] S. Hashemi, Finding topological charges in confined ellipses, *Braz. J. Phys.* **49**, 44 (2019).
- [42] S.-H. Suh, B.-D. Jung, Y.-J. Park, V. Chihaiia, V. Parvulescu, and M. Gartner, Simulation studies for random sequential adsorption in narrow slit: Two-dimensional parking model, *Bull. Korean Chem. Soc.* **29**, 873 (2008).
- [43] A. Rényi, On a one-dimensional problem concerning random space filling, *Select. Transl. Math. Stat. Probab.* **4**, 203 (1963) [translation from Magyar Tud. Akad. Mat. Kutató Int. Közl. 3, No. 1-2, 109 (1958)].
- [44] S. C. van der Marck, Percolation thresholds and universal formulas, *Phys. Rev. E* **55**, 1514 (1997).
- [45] J. Hoshen and R. Kopelman, Percolation and cluster distribution. I. Cluster multiple labeling technique and critical concentration algorithm, *Phys. Rev. B* **14**, 3438 (1976).
- [46] N. G. Almarza, C. Martín, and E. Lomba, Phase behavior of the hard-sphere Maier-Saupe fluid under spatial confinement, *Phys. Rev. E* **80**, 031501 (2009).
- [47] Y. Mao, P. Bladon, H. N. W. Lekkerkerker, and M. E. Cates, Density profiles and thermodynamics of rod-like particles between parallel walls, *Mol. Phys.* **92**, 151 (1997).
- [48] M. Dijkstra, R. van Roij, and R. Evans, Wetting and capillary nematization of a hard-rod fluid: A simulation study, *Phys. Rev. E* **63**, 051703 (2001).
- [49] D. de las Heras, E. Velasco, and L. Mederos, Capillary effects in a confined smectic phase of hard spherocylinders: Influence of particle elongation, *Phys. Rev. E* **74**, 011709 (2006).
- [50] M. Aghaei Semiromi and A. Avazpour, Computer simulation of confined prolate hard spherocylinder liquids between hard walls, *Liq. Cryst.* **45**, 262 (2018).
- [51] A. Chrzanowska, P. I. C. Teixeira, H. Ehrentraut, and D. J. Cleaver, Ordering of hard particles between hard walls, *J. Phys.: Condens. Matter* **13**, 4715 (2001).
- [52] A. Malijevsky and S. Varga, Phase behaviour of parallel hard rods in confinement: An Onsager theory study, *J. Phys.: Condens. Matter* **22**, 175002 (2010).
- [53] S. M. Ghazi, F. Behzadi, and R. Aliabadi, Second-virial Onsager theory and its limitations in the prediction of the ordering transitions of confined hard rods between two parallel hard walls, *J. Phys. Soc. Jpn.* **89**, 114601 (2020).
- [54] E. Basurto, P. Gurin, S. Varga, and G. Odriozola, Anisotropy-independent packing of confined hard ellipses, *J. Mol. Liq.* **333**, 115896 (2021).
- [55] Z. Adamczyk, K. Jaszczólt, A. Michna, B. Siwek, L. Szyk-Warszyńska, and M. Zembala, Irreversible adsorption of particles on heterogeneous surfaces, *Adv. Colloid Interface Sci.* **118**, 25 (2005).
- [56] N. Aggarwal, K. Lawson, M. Kershaw, R. Horvath, and J. Ramsden, Protein adsorption on heterogeneous surfaces, *Appl. Phys. Lett.* **94**, 083110 (2009).
- [57] M. Sadowska, M. Cieśla, and Z. Adamczyk, Nanoparticle deposition on heterogeneous surfaces: Random sequential adsorption modeling and experiments, *Colloids Surf., A* **617**, 126296 (2021).